Arch. Mech., **67**, 4, pp. 293–310, Warszawa 2015

Enhancement of bending fatigue life in TiNi shape-memory alloy tape by nitrogen ion implantation

K. TAKEDA[1)], R. MATSUI[1)], H. TOBUSHI[1)], S. HOMMA[2)], N. LEVINTANT-ZAYONTS[3)], S. KUCHARSKI[3)]

[1)] *Department of Mechanical Engineering*
Aichi Institute of Technology
1247 Yachigusa, Yakusa-cho, Toyota 470-0392, Japan
e-mails: k-takeda@aitech.ac.jp, r_ matsui@aitech.ac.jp, tobushi@aitech.ac.jp

[2)] *Nippon Trex Co., Ltd.*
350 Minamiyama Shinden
Ina-cho, Toyokawa 441-0193, Japan
e-mail: 1031homma1031@gmail.com

[3)] *Institute of Fundamental Technological Research*
Polish Academy of Sciences
Pawinskiego 5B, 02-106 Warsaw, Poland
e-mails: neonila@ippt.pan.pl, skuchar@ippt.pan.pl

A SHAPE-MEMORY ALLOY (SMA) is expected to be applied as intelligent or smart material since it shows the functional characteristics of the shape memory effect and superelasticity. Most SMA elements, with these characteristics, perform cyclic motions. In these cases, the fatigue property of SMA is one of the most important issues in view of evaluating functional characteristics of SMA elements. The fatigue properties are complex since they depend on stress, strain, temperature and their hysteresis. If an SMA is implanted with high-energy ions, the thermomechanical properties of the material may change, resulting in long fatigue life. In the present study, the nitrogen ion implantation was applied to modify the surface of a TiNi SMA tape and the influence of implantation treatment on the bending fatigue properties was investigated.

Key words: shape-memory alloy, titanium-nickel alloy, superelasticity, nitrogen ion implantation, fatigue, bending.

1. Introduction

THE SHAPE-MEMORY ALLOY (SMA) is expected to be applied as intelligent material since it shows the unique characteristics of the shape memory effect and superelasticity (pseudoelasticity) [1]. The TiNi SMAs are most widely used in practical applications of SMAs since their fatigue life is longer, their recoverable

strain is larger and their corrosion resistance is higher than in other SMAs. In the growing number of TiNi SMA applications, these materials should fulfill high requirements of resistance to fatigue, corrosion and wear. On the other hand, the application of SMA has some limitations, particularly in thermomechanical cyclic loading cases, when structural components can be damaged due to fatigue [2–4]. In these cases, fatigue of SMA is one of the important properties in view of evaluating functional characteristics of SMA elements.

In general, the ion implantation process may be used to improve the mechanical properties of surface that lead to longer fatigue life in cyclic-thermomechanical loading conditions as well as higher resistance to corrosion and wear [5, 6]. It is known that ion implantation is a surface engineering process where ions of different materials are accelerated in electron field and penetrate into a near-surface region of a solid. The ion implantation process is used to change the physical, chemical or electrical properties of solids [5]. In this process, a large number of ions bombard a surface, penetrate in near-surface region interacting with the substrate atoms and a thin surface layer is generated having different properties than the bulk materials. In surface engineering, the above process is applied to improve mechanical properties such as hardness, wear and fatigue resistance [7–10].

In the previous paper [11], the nitrogen ion was implanted into a TiNi SMA wire from two opposite directions and the influence of ion-implantation treatment on the bending fatigue properties was investigated. It was confirmed that the fatigue life becomes longer due to ion implantation. However, in the case of wires, ion is not uniformly implanted into the cylindrical surface layer of the wire.

In the present paper, the influence of nitrogen ion implantation on the tensile deformation, bending fatigue life, hardness and surface roughness was investigated for a TiNi SMA tape.

2. Experimental method

2.1. Materials and specimen

The materials used in the experiment were Ti-50.85at%Ni tapes with a thickness of 1 mm and a width of 2.5 mm. The length of the tapes was 80 mm for the tensile test and 100 mm for the fatigue test. They were polycrystalline, produced by Furukawa Techno Material Co., Ltd. and applied to an element of a brassiere. The tapes were heat-treated at 803 K for 10 min followed by water quenching. The transformation temperatures M_s, M_f, R_s, R_f, A_s and A_f of the material were 248, 178, 312, 262, 250 and 322 K, respectively. The material shows therefore superelasticity at room temperature.

2.2. Nitrogen ion implantation

The surface of as-received tape samples was polished by using 1000, 1200, 1500, 2000 and 2500 grit sandpaper (abrasive paper) and then finished by using 0.04 micrometer (μm) SiO_2 colloidal suspension. The surface of the polished tape-samples was cleaned using alcohol and hot acetylene. TiNi SMA tape-samples were gripped into place in special holders that enabled the ion beam treatment of the two opposite sides. The TiNi SMA tape was ion-implanted from two opposite directions by nitrogen ion beam. Nitrogen ion implantation was carried out using semi-industrial implanter IMJON (Institute of Fundamental Technological Research, Polish Academy of Sciences, Warsaw). The energy of nitrogen ion beam was 50 keV and three doses of nitrogen ions were applied: 8×10^{16}, 3×10^{17} and 2.5×10^{18} ions/cm^2. The surface color of the ion-implanted tape with 2.5×10^{18} ions/cm^2 is of deeper gold than that with 8×10^{16} ions/cm^2. The temperature of TiNi samples during the ion implantation treatment was measured using thermocouple. The temperature of the samples starts from room temperature, then monotonically increases and at the end of implantation process it reaches the values of 353, 413 and 503 K for doses of 8×10^{16}, 3×10^{17} and 2.5×10^{18} ions/cm^2, respectively.

The applied nitrogen ion fluences result from observation made by other authors. The 10^{16} ions/cm^2 dose is considered as the lowest dose that influences the mechanical properties of metals [12, 13]. The medium dose 10^{17} ions/cm^2 was applied in different papers and it has been shown that it improves hardness, wear and corrosion resistance as well as fatigue life of metals [10, 14]. The dose of range of 10^{18} ions/cm^2 in turn corresponds to the highest doses of nitrogen ions implanted into metals, described in [15, 16]. Some observations indicate that such high number of doses leads to deterioration of mechanical properties. The goal of our experiment is to verify if whether the 10^{18} ions/cm^2 nitrogen dose could still improve the fatigue life of NiTi SMA. As there are no many papers concerning number of ion implantation of TiNi SMA, the implanted ion doses are in the range of the lowest and highest doses applied to metals. In this paper, we have not considered the chemical composition of the implanted layer. Instead, we have focused on final mechanical effects of ion implantation treatment. The microstructure and chemical composition of nitrogen implanted layers on TiNi SMA possessing slightly different composition from the alloy investigated in this study were shown in other papers [17, 18]. The ion energy in our experiments corresponds to mean energy applied in semi-industrial implanter machines [5, 6] and influence of ion beam energy variation was not considered.

We have not observed a change of roughness due to ion implantation treatment. The different values of roughness observed for different implantation doses can be a result of randomness of polishing process rather than the effect of implanted ions.

2.3. Tensile test

In the tensile test, displacement was measured by an extensometer with a gauge length of 50 mm for the specimen. Strain ε was determined by nominal strain. The tensile test was carried out under a constant strain rate $d\varepsilon/dt = 1.67 \times 10^{-4}$ s^{-1} in air at room temperature (RT).

2.4. Fatigue test

In the fatigue test, an alternating-plane bending fatigue test machine [19] was used. The test for alternating-plane bending fatigue was carried out in air at room temperature. The maximum bending strain appeared on the flat surface where the ion implantation was applied. The frequency of cyclic bending was found to be 2.5 Hz (150 cpm). A scanning electron microscope (SEM) was used to observe the fracture surface of the specimen.

2.5. Nanoindentation test

The CSM Open Platform equipment used to perform indentation tests is described briefly. The ultra-nano indenter UNHT was used in nano scale to measure load-penetration curves of the non-implanted and ion-implanted samples. In the nano system, the maximum penetration depth is $h = 50$ μm and load range is $F = 0$–50 mN (standard range). The displacement resolution and load resolution are 0.0005 nm and 2.5 nN, respectively. The thermal drift equals 0.5 nm/min. A Berkovich diamond indenter tip was used.

3. Results and discussion

3.1. Tensile deformation properties

The stress-strain curves of five kinds of SMA tapes: as-received, polished, ion-implanted with 8×10^{16}, 3×10^{17} and 2.5×10^{18} ions/cm^2, obtained by the tensile test are shown in Fig. 1. All stress-strain curves draw hysteresis loops during loading and unloading, showing the superelasticity. In the case of ion-implanted with 2.5×10^{18} ions/cm^2, the residual strain of 1% appears after unloading, showing the partial superelasticity. This residual strain disappears by heating under no-load, showing the shape memory effect. The upper stress plateau during loading appears due to the stress-induced martensitic transformation. The lower stress plateau during unloading appears due to the reverse transformation. The martensitic transformation stress σ_M and the reverse transformation stress σ_A decrease markedly in the case of ion-implanted with 2.5×10^{18} ions/cm^2 compared to other conditions. Although the ion-implanted region is limited in the surface layer, temperature of the tape increases during the ion implantation

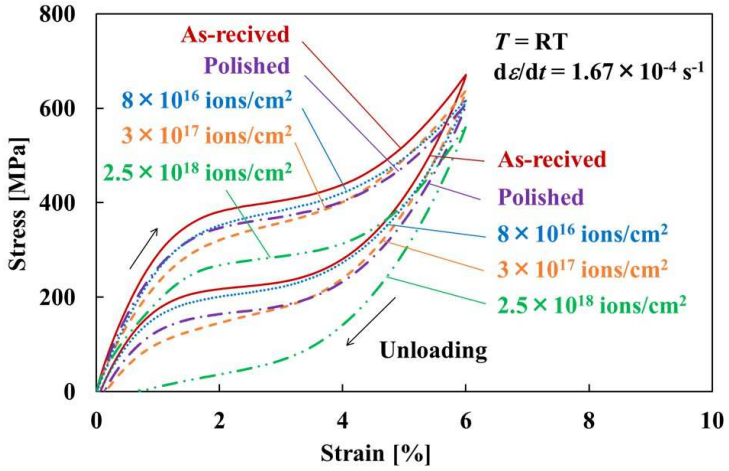

FIG. 1. Stress-strain curves.

process. If the shape memory processing temperature is high, both transformation stresses decrease [20]. The same as in the shape memory processing, the transformation stresses therefore decrease due to the temperature rise during the ion implantation process. In the case of ion-implanted with 8×10^{16} and 3×10^{17} ions/cm^2, the transformation stress decreases slightly compared to that of the as-received tape.

3.2. Bending fatigue property

3.2.1. Fatigue life

(1) *Fatigue life curve.* The relationships between the bending strain amplitude ε_a and the number of cycles to failure N_f for five kinds of tapes obtained by the alternating-plane bending fatigue test under a constant frequency $f = 150$ cpm at room temperature are shown in Fig. 2. The bending strain amplitude ε_a was obtained from the bending strain on the surface of the specimen at fracture point. The specimen was fractured at the midpoint of two grips. As can be seen in Fig. 2, the larger the bending strain amplitude, the shorter the fatigue life is. The fatigue life of the polished and ion-implanted tapes is longer than that of the as-received tape. The fatigue life with 8×10^{16} ions/cm^2 is close to that of the polished tape. The fatigue life with 2.5×10^{18} ions/cm^2 is longer than that of other ion-implanted tapes, and is 7.5 times longer than that of the as-received tape.

The relationships between the bending strain amplitude ε_a and the number of cycles to failure N_f shown on the logarithmic graph are almost expressed by straight lines for all materials. The relationship can be therefore expressed by

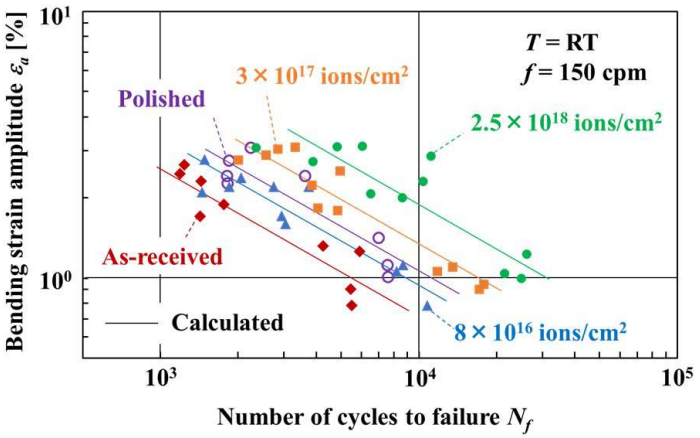

FIG. 2. Relationship between bending strain amplitude and the number of cycles to failure.

a power function as follows:

$$\varepsilon_a \cdot N_f^{\beta} = \alpha, \tag{3.1}$$

where α and β represent ε_a in $N_f = 1$ and the slope of the $\log \varepsilon_a - \log N_f$ curve, respectively. The values of $\beta = 0.55$ are almost the same for all tapes. The values of α are 1.16, 1.68, 1.49, 2.09 and 3.04 for as-received, polished and ion-implanted with 8×10^{16}, 3×10^{17} and 2.5×10^{18} ions/cm^2, respectively. The calculated results of Eq. (3.1) are marked as solid lines in Fig. 2. The overall inclinations are well approximated by the solid lines. The dependence of α on the amount of ion implantation will be discussed in Section 3.3.

(2) *Temperature rise.* During cyclic bending, the surface of the TiNi SMA tape is subjected to the interface friction between the martensitic variant and austenite phase repeatedly. Temperature of the material therefore increases markedly during the early 20–30 cycles and it saturates thereafter at a certain value [21]. Temperature of the specimen surface at the midpoint of two grips, where the maximum bending strain appeared, was measured by a thermocouple during the alternating-plane bending fatigue test. The relationships between the saturated temperature rise ΔT_S and the bending strain amplitude ε_a for five kinds of tapes obtained from the test at room temperature (RT) are shown in Fig. 3. In Fig. 3, the obtained data are plotted with several symbols for each tape. The region, where the data are plotted, is shaded. Temperature rise ΔT_S increases in proportion to ε_a for all tapes. The values of ΔT_S for the as-received tape are slightly larger than those for other tapes. As seen in Fig. 1, the stress-strain curve of the tape draws a hysteresis loop during loading and unloading. The area surrounded by the hysteresis loop corresponds to the dissipated work per unit volume W_d [22]. The dissipated work W_d is evaluated by the product

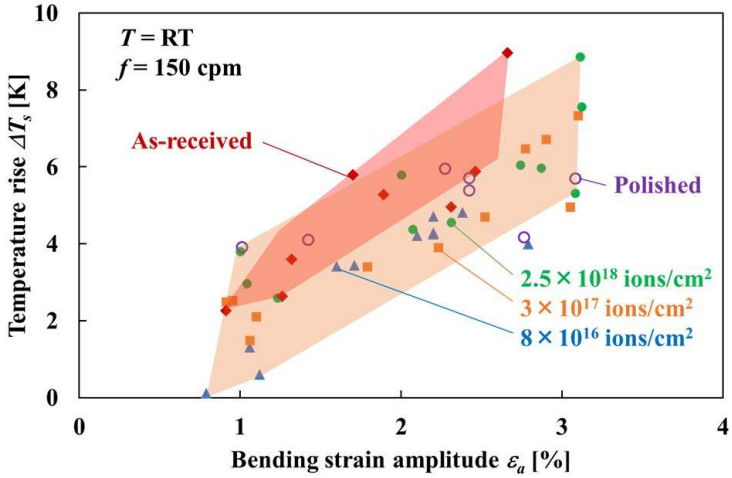

FIG. 3. Relationship between saturated temperature rise ΔT_s and bending strain amplitude ε_a.

of the difference $(\sigma_M - \sigma_A)$ between the upper plateau stress σ_M and the lower plateau stress σ_A and the martensitic transformation strain range ε_M. The dissipated work W_d of the surface element with the bending strain amplitude ε_a is estimated by the following equation [23]:

$$W_d = (\sigma_M - \sigma_A)(\varepsilon_a - \varepsilon_{MS}), \tag{3.2}$$

where ε_{MS} denotes the martensitic transformation start strain. Therefore, if ε_a is large, W_d is large, and as a result large amount of heat is generated. This is the reason why ΔT_S increases in proportion to ε_a. In SMAs, σ_M increases in proportion to temperature T as follows: $d\sigma_M/dT = C_M$ and $C_M = 6$ MPa/K for TiNi SMA [24]. Therefore, if ΔT_S is large, σ_M increases. It should be noticed that, in the practical application of SMA elements, high σ_M induced due to temperature rise ΔT_S under cyclic bending causes large fatigue damage, resulting in short fatigue life.

3.2.2. Fatigue crack

(1) *Fracture surface.* In the case of most as-received tapes, the fatigue crack initiates at the central part of the flat surface subjected to maximum bending strain. On the other hand, in the case of all polished tapes and most ion-implanted tapes, the fatigue crack initiates at the round corner on the side near the flat surface. Let us discuss the influence of polishing and ion-implantation on the fatigue crack initiation and the fatigue crack growth by observing the fracture surface.

(i) *As-received tape.* Figure 4 shows the SEM photograph of a typical fracture surface of the as-received tape obtained by the fatigue test for $\varepsilon_a = 2.46\%$. In Fig. 4, F_c denotes the point of the fatigue crack initiation. The crack nucleates at a certain point F_c in the central part of the flat surface of eight tapes out of nine tapes and propagates toward the center in a sinuous radial pattern. Although small cracks are observed in both flat surfaces of the tape subjected to maximum bending strain, one single crack grows preferentially. Following the appearance of fatigue crack with a semi-elliptical surface, unstable fracture finally occurs. In the case of the as-received tape, the point F_c appears at a central part of the flat surface and the fatigue life is short.

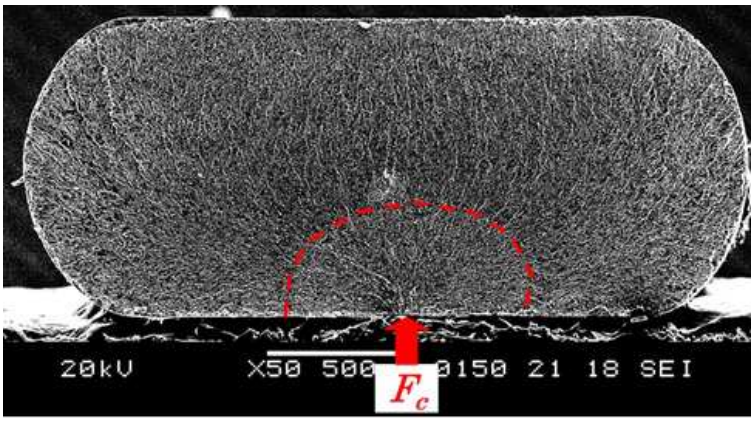

FIG. 4. SEM photograph of the typical fracture surface of as-received tape for $\varepsilon_a = 2.46\%$ and $N_f = 1185$.

(ii) *Polished tape.* Figure 5 shows the SEM photograph of a typical fracture surface of the polished tape obtained by the fatigue test for $\varepsilon_a = 2.42\%$. In Fig. 5, F_c denotes the point of the fatigue crack initiation. As can be seen in Fig. 5, the fatigue crack nucleates at a certain point F_c at the round corner on the side near the flat surface of eight tapes out of eight tapes and propagates toward the center in a sinuous radial pattern. The distance from the flat surface of the tape to the crack initiation point F_c is 35 μm. Although small cracks are observed on four corner surfaces of the tape, one single crack grows preferentially. The reason why the fatigue crack nucleates on the corner surface is as follows. Although the maximum bending strain appears on the flat surface of the tape, the flat surface is polished and the surface is smooth, and it is therefore hard for the fatigue crack to nucleate on the flat surface. The side of the tape is not polished and the surface is therefore rough. As a result, the fatigue crack nucleates at the point F_c on the side near the flat surface. In practical applications of SMAs, the fatigue life of SMA elements increases if the surface is polished not only on the

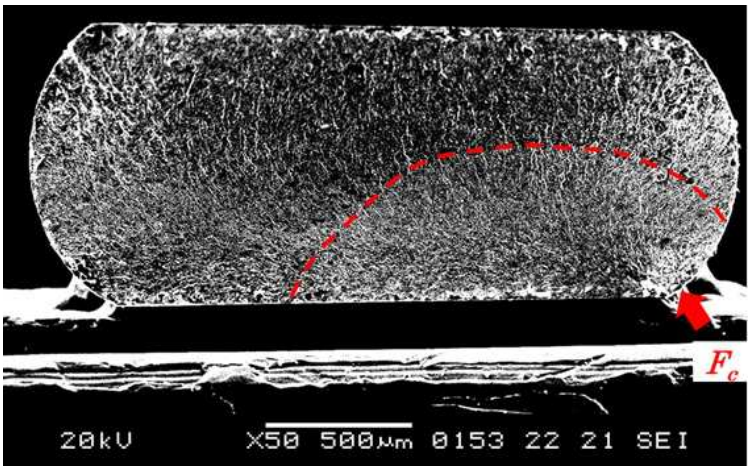

FIG. 5. SEM photograph of the typical fracture surface of polished tape for $\varepsilon_a = 2.42\%$ and $N_f = 3615$.

surface at the maximum stress point but also on the surface in the region near the maximum stress point. The detail of the observed-surface roughness will be discussed in Section 3.2.4.

(iii) *Ion-implanted tapes.* SEM photographs of a typical fracture surface for the ion-implanted tape with 2.5×10^{18} ions/cm^2 in the case of a bending strain amplitude $\varepsilon_a = 3.12\%$ are shown in Fig. 6. The whole fracture surface, the fracture surface in the crack initiation part (1), the fracture surface in the middle part of unstable fracture region (2), and the fracture surface in the final unstable fracture part (3) located on the opposite side of the crack initiation part (1) are shown in Figs. 6a, 6b, 6c and 6d, respectively.

As can be seen in Figs. 6a and 6b, the fatigue crack nucleates at a certain point F_c in the round corner part (1) on the side near the flat surface of 26 tapes out of 34 tapes and propagates toward the center in a sinuous radial pattern. The distance from the flat surface of the tape to the crack initiation point F_c is 30 μm. Although small cracks are observed on four corner surfaces of the tape, one single crack grows preferentially. The reason why the fatigue crack nucleates on the corner surface is as follows. Although the maximum bending strain appears on the flat surface of the tape, the flat surface is smooth and hardness of the surface is high due to the ion implantation, and it is therefore hard for the fatigue crack to nucleate on the flat surface. The side surface of the tape is subjected to slight ion implantation. As a result, the fatigue crack nucleates at the point F_c near the flat surface. This phenomenon is similar to the fatigue crack initiation point of a TiNi SMA wire subjected to nitrogen ion implantation [11]. In the case of

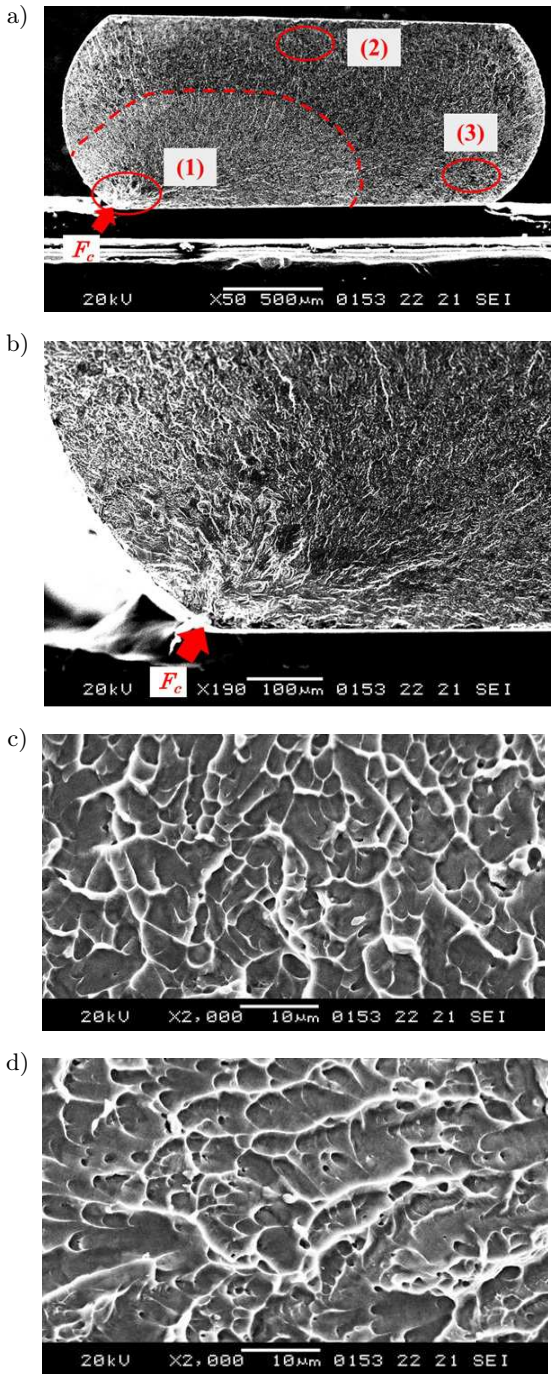

FIG. 6. SEM photographs of the typical fracture surface of ion-implanted tape with 2.5×10^{18} ions/cm^2 for $\varepsilon_a = 3.12\%$ and $N_f = 6018$: a) whole fracture surface, b) crack initiation part (1), c) central fracture part (2), d) final fracture part (3).

the ion-implanted wire, the fatigue crack nucleates at a certain point different from the maximum bending strain point where the maximum amount of nitrogen ion was implanted. In practical applications of SMAs, the fatigue life of SMA elements increases if the nitrogen ion is implanted not only on the surface at the maximum stress point but also on the surface in the region near the maximum stress point.

As can be seen in Fig. 6a, following the appearance of fatigue fracture with a quarter-elliptical surface, unstable fracture finally occurs. As can be seen in Fig. 6c, isometric dimples with an average diameter of about 3 μm appear in the middle part of unstable fracture region (2). As seen in Fig. 6d, elongated dimples are found distributed in the direction parallel to the flat surface according to the propagation of the crack induced by tearing in the final unstable fracture part (3).

(2) *Fatigue crack growth*

(i) *Fatigue crack growth area.* Let us discuss the fatigue crack growth area A_f which is surrounded by the dashed semi-elliptical or quarter-elliptical lines shown in Figs. 4, 5 and 6(a). The relationships between the fatigue crack growth area A_f and the bending strain amplitude ε_a for five kinds of tapes obtained by the fatigue test are shown in Fig. 7. In Fig. 7, the obtained data are plotted with several symbols for each tape. The regions, where the data are plotted, are shaded separately for the ion-implanted tape with 2.5×10^{18} ions/cm^2 and for other four tapes. As can be seen in Fig. 7, only the area A_f of the ion-implanted tape with 2.5×10^{18} ions/cm^2 is larger than that of other four tapes. The larger the bending strain amplitude, the smaller the fatigue crack growth

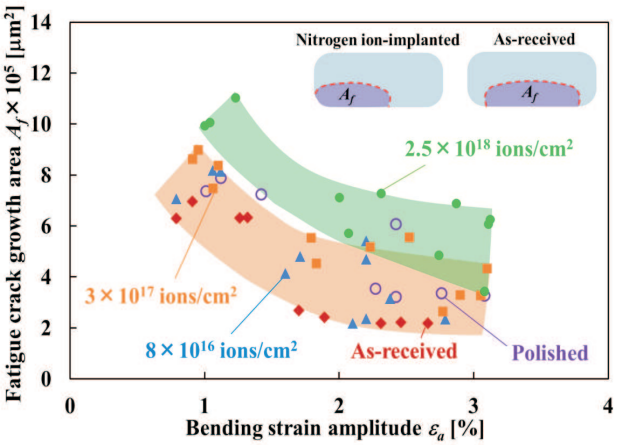

FIG. 7. Relationship between fatigue crack growth area and bending strain amplitude.

area is. If the bending strain amplitude is large, the fatigue crack growth area is small, resulting in a short fatigue life. In the case of ion implantation with 2.5×10^{18} ions/cm^2, A_f is larger than other conditions, which corresponds to the longer fatigue life.

(ii) *Fatigue crack growth length.* As observed in Figs. 4 and 6(a), the fatigue fracture region shows a semi-elliptical or a quarter-elliptical form. Let us discuss the fatigue crack growth length along the flat surface a_s from the crack initiation point F_c and that toward the center a_c. The dependence of a_s and a_c on the bending strain amplitude ε_a is shown in Fig. 8. In Fig. 8, the data of a_s are plotted as closed symbols and the data of a_c as open symbols, respectively. The regions, where they are plotted, are shaded. As can be seen, the larger the bending strain amplitude ε_a, the smaller the crack growth length a_s . The values of a_s for the as-received tape are smaller than those for the ion-implanted tapes, which corresponds to the shorter fatigue life of the as-received tape. The dependence of a_c on ε_a is slight. Values of a_c are about 0.5 mm, a half of a thickness of the tape of 1 mm. Values of a_s are larger than those of a_c since the bending strain is largest on the flat surface of the tape and small in the central part of the tape.

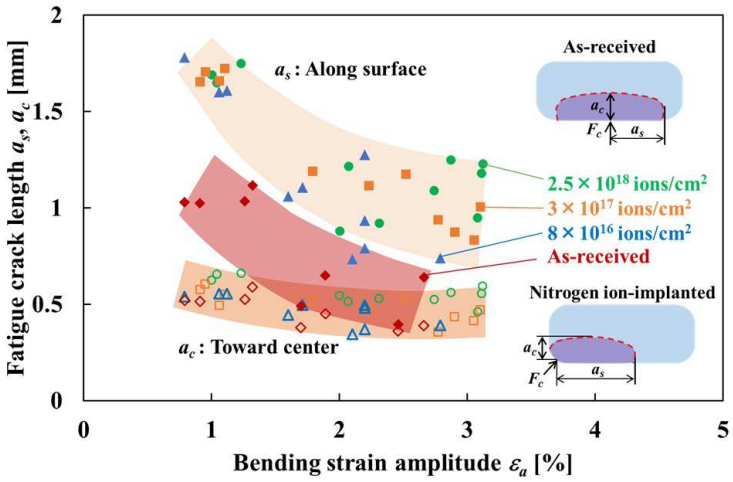

FIG. 8. Dependence of fatigue crack lengths a_s and a_c on bending strain amplitude: a_s is shown by closed symbols and a_c by open symbols.

(iii) *Average fatigue crack growth rate.* The dependence of average fatigue crack growth rate till fracture along the flat surface a_s/N_f and the one toward the center a_c/N_f on the bending strain amplitude ε_a for the as-received tape and the ion-implanted tape with 2.5×10^{18} ions/cm^2 is shown in Fig. 9. In Fig. 9, the data of a_s/N_f are plotted as closed symbols and those of a_c/N_f as open

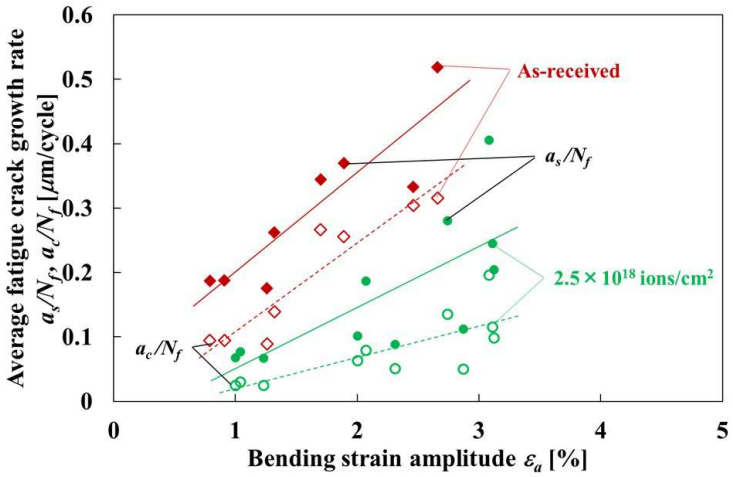

FIG. 9. Dependence of average fatigue crack growth rates a_s/N_f and a_c/N_f on bending strain amplitude ε_a for tapes as-received and ion-implanted with 2.5×10^{18} ions/cm^2: a_s/N_f is shown by closed symbols and a_c/N_f by open symbols.

symbols, respectively. As can be seen, the larger the bending strain amplitude, the larger the crack growth rates. The rate a_s/N_f is higher than a_c/N_f. The average fatigue crack growth rates for the as-received tape are higher than those for the ion-implanted tape. This means that the average fatigue crack growth rates decrease by the ion implantation, resulting in longer fatigue life.

3.2.3. Influence of hardness on fatigue life

Hardness of the surface for SMA tapes was measured by the nano-indentation test using the Oliver-Pharr method [25]. In the test, the load of 1.5 and 2 mN was applied and the total penetration depth did not exceed 140 nm. The relationships between the number of cycles to failure N_f and hardness H for various values of bending stain amplitude ε_a are shown in Fig. 10. In Fig. 10, the data are plotted with several symbols. As can be seen in Fig. 10, the fatigue life N_f increases in proportion to hardness H for each ε_a. The relationships shown on the semi-logarithmic graph are expressed by almost straight lines for each ε_a and can be therefore expressed by the following equation:

$$\log_{10} N_f = \log_{10} a + bH, \tag{3.3}$$

where a and b represent N_f in $H = 0$ and the slope of the $\log_{10} N_f - H$ curve, respectively. The fatigue life N_f can be expressed by an exponential function of H from Eq. (3.3) as follows:

$$N_f = ae^{\ln 10 \cdot bH}. \tag{3.4}$$

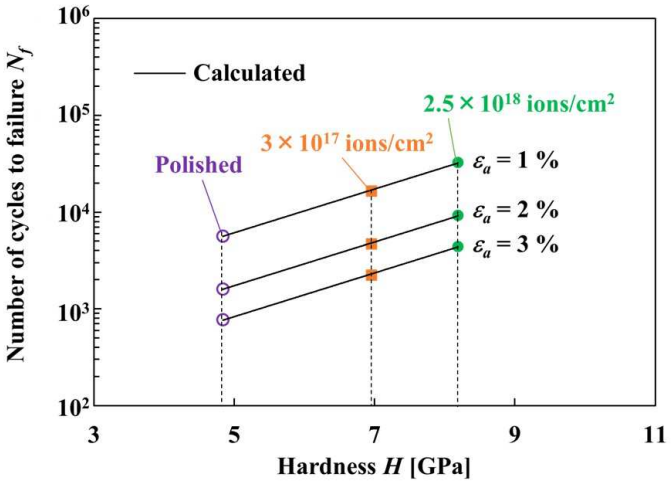

FIG. 10. Relationship between number of cycles to failure N_f and hardness H in thin surface layer obtained from nanoindentation test.

The straight lines for each ε_a are almost parallel, that is, the slope b is the same for all ε_a and $b = 2.26 \times 10^{-10}$ Pa^{-1}. The coefficient a can be expressed by an exponential function of ε_a as follows:

$$a = 113e^{-43.6\varepsilon_a}. \tag{3.5}$$

The results calculated from Eqs. (3.4) and (3.5) are depicted by solid lines in Fig. 10. The overall inclinations are well-approximated by the solid lines.

3.2.4. Surface roughness

It is known that surface roughness of the material affects the fatigue life. If the surface is rough, the fatigue life is short [26]. In order to investigate the influence of surface roughness on the fatigue life, surface roughness was measured.

Arithmetic mean roughness R_a for five kinds of tapes is shown in Fig. 11. The value of R_a for the as-received tape is 0.65 μm. The values of R_a for the polished and ion-implanted tapes are 0.15–0.25 μm. The influence of the ion-implantation on the surface roughness is therefore small. The values of R_a for the polished and ion-implanted tapes are about one-third as large as that of the as-received tape. As seen in Fig. 2, the fatigue life of the polished and ion-implanted tapes is longer than that of the as-received tape. Therefore, if the surface is smooth, the fatigue life is long.

3.3. Influence of ion implantation on σ_M and α

Let us discuss the influence of ion implantation on the tensile deformation property and fatigue life. As observed in previous sections, if high dose of nitrogen

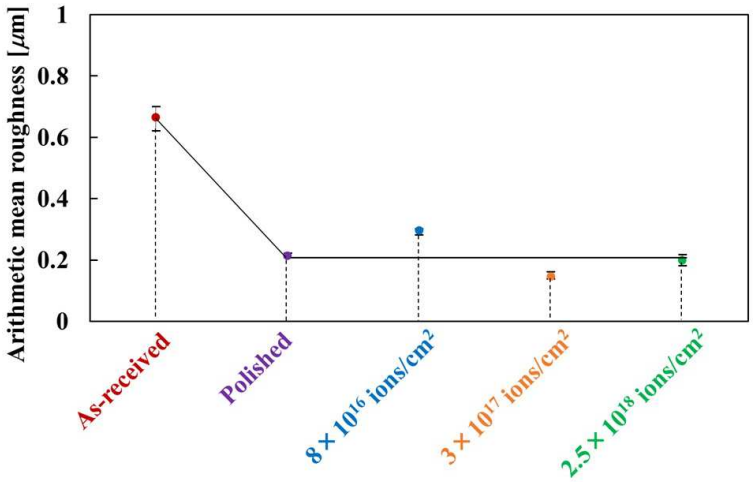

FIG. 11. Arithmetic mean surface roughness for five kinds of materials.

ion is applied, the upper plateau stress σ_M decreases (Fig. 1) and the strain amplitude α at $N_f = 1$ on the fatigue life curve increases (Fig. 2 and Eq. (3.1)). The dependence of σ_M and α on the dose of ion implantation I_n obtained by the experiments is shown in Fig. 12. The upper plateau stress σ_M was obtained from the intersection of two straight lines: the line with the initial elastic slope of the stress-strain curve and that with the slope of the upper stress plateau region. Both relationships are shown by almost straight lines. The relationships can be

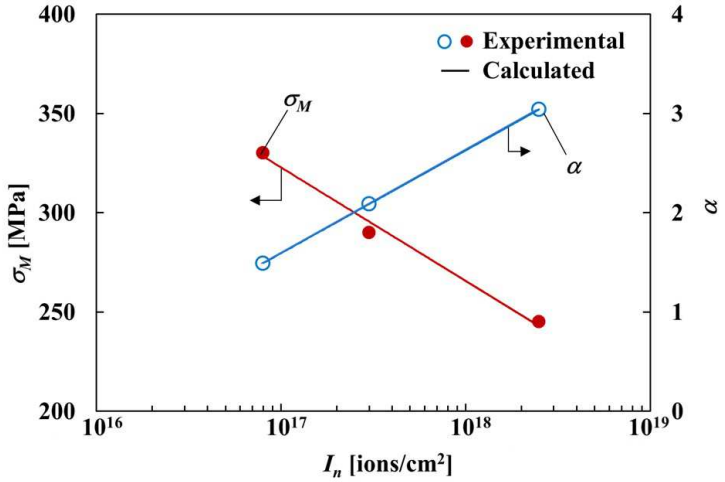

FIG. 12. Dependence of σ_M and α on I_n.

therefore expressed by the following equations:

$$\begin{aligned} \sigma_M &= -56.9 \log_{10} I_n + 1294, \\ \alpha &= 1.04 \log_{10} I_n - 16. \end{aligned} \tag{3.6}$$

The calculated results of Eq. (3.6) are marked as solid lines in Fig. 12. The overall inclinations are well-approximated by the solid lines.

4. Conclusions

The nitrogen ion was implanted into a TiNi SMA tape, in which both flat surfaces were ion-implanted from two opposite directions, and the influence of the nitrogen ion implantation on the fatigue life of alternating-plane bending was investigated. The results obtained are summarized as follows.

1. The larger the bending strain amplitude, the shorter the fatigue life. The fatigue life of the ion-implanted tape is longer than that of the as-received tape. The fatigue lives of both the polished tape and the ion-implanted tape with 8×10^{16} ions/cm^2 are almost the same. The fatigue life of the ion-implanted tape with 2.5×10^{18} ions/cm^2 is longer than that with 8×10^{16} and 3×10^{17} ions/cm^2.
2. The fatigue crack nucleates at the central part of the flat surface of the as-received tape. The fatigue crack nucleates at the round corner on the surface near the flat surface of the polished and ion-implanted tapes. The larger the bending strain amplitude, the smaller the fatigue crack growth area. The fatigue crack growth length along the surface is longer than the one toward the center. The average fatigue crack growth rate increases in proportion to the bending strain amplitude and decreases by the ion implantation.
3. The hardness on the surface of the tape increases by the ion implantation. The fatigue life increases in proportion to the hardness on the surface of the tape for each bending strain amplitude.
4. The influence of the ion implantation on the surface roughness is slight. The fatigue life of the polished and ion-implanted tapes with smooth surface is longer than that of the as-received tape with rough surface.
5. In practical applications of SMAs, the fatigue life of SMA elements increases if the nitrogen ion is implanted not only on the surface at the maximum stress point but also on the surface in the region near the maximum stress point.

Acknowledgement

The experimental work for this study was carried out with the assistance of students in Aichi Institute of Technology, to whom the authors wish to express their gratitude. The authors also wish to extend thanks to the administrators of scientific research in Grants-in-Aid for Scientific Research (C) (General) by the Japan Society for the Promotion of Science for financial support. This work was also partially supported by the Polish National Science Center Project 2013/09/D/ST8/04011.

References

1. K. Otsuka, C.M. Wayman [Eds.], *Shape Memory Materials*, Cambridge University Press, Cambridge, 1998, 1–49.
2. M. Wagner, T. Sawaguchi, G. Kaustrater, D. Hoffken, G. Eggeler, *Structural fatigue of pseudoelastic NiTi shape memory wires*, Materials Science and Engineering A, **378**, 105–109, 2004.
3. R. Matsui, H. Tobushi, Y. Furuichi, H. Horikawa, *Tensile deformation and rotating-bending fatigue properties of a high-elastic thin wire, a superelastic thin wire, and a superelastic thin tube of NiTi alloys*, Trans. ASME, J. Eng. Mater. Tech., **126**, 384–391, 2004.
4. H. Tobushi, R. Matsui, K. Takeda, E.A. Pieczyska, *Mechanical properties of shape memory materials. Part 2: Fatigue properties of shape-memory alloy*, Nova Science Pub., New York, 2013, 115–164.
5. J.K. Hirvonen, *Ion Implantation*, Academic Press, United States, 1980.
6. I.P. Jain, G. Agarwal, *Ion beam induced surface and interface engineering*, Surface Science Reports, **66**, 77–172, 2011.
7. T. Asaoka, M. Mitsuo, *Effect of aluminum ion implantation on shape-memory properties of titanium-nickel alloy*, Materials Transactions, JIM, **41**, 6, 739–744, 2000.
8. H. Peletier, D. Muller, P. Mille, J. Grob, *Structural and mechanical characterization of born and nitrogen implanted NiTi shape memory alloy*, Surface and Coating Technology, **158-159**, 309–317, 2002.
9. A.D. Pogrebnjak, E.A. Bazyl, *Modification of wear and fatigue characteristics of Ti-V-Al alloy by Cu and Ni ion implantation and high-current electron beam treatment*, Vacuum, **64**, 1, 1–7, 2001.
10. L. Fengbin, F. Guohao, C. Yan, S. Qiguo, Q. Min, S. Yi, *Tribological properties and surface structures of ion implanted 9Cr18Mo stainless steels*, Nuclear Instruments and Methods in Physics Research B, **307**, 412–418, 2013.
11. K. Takeda, K. Mitsui, H. Tobushi, N. Levintant-Zayonts, S. Kucharski, *Influence of nitrogen ion implantation on deformation and fatigue properties of TiNi shape memory alloy wire*, Arch. Mech. **65**, 5, 391–405, 2013.
12. L.D. Yu, G.W. Shuy, T. Vilaithong, *Friction modification of WC-Co by ion implantation*, Surface and Coatings Technology, **128-129**, 404–409, 2000.

13. L. THAIR, U. KAMACHI MUDALI, N. BHUVANESWARAN, K.G. NAIR, R. ASOKAMANI, B. RAJ, *Nitrogen ion implantation and in vitro corrosion behavior of as-cast Ti–6Al–7Nb alloy*, Corrosion Science, **44**, 2439–2457, 2002.

14. P.W. SHUM, Y.F. XU, Z.F. ZHOU, W.L. CHENG, K.Y. LI, *Study of TiAlSiN coatings post-treated with N and C+N ion implantations. Part 2: the tribological analysis*, Wear, **274-275**, 274–280, 2012.

15. D. MANOVA, D. HIRSCH, E. RICHTER, S. MÄNDL, H. NEUMANN, B. RAUSCHENBACH, *Microstructure of nitrogen implanted stainless steel after wear experiment*, Surface & Coatings Technology, **201**, 8329–8333, 2007.

16. S. GOKUL LAKSHMI, D. ARIVUOLI, *Enhanced wear resistance of Ti-5Al-2Nb-1Ta orthopedic alloy by nitrogen ion implantation*, Tribology International, **39**, 548–552, 2006.

17. N. LEVINATNT-ZAYONTS, S. KUCHARSKI, *Surface characterization and wear behavior of ion-implanted NiTi shape memory alloy*, Vacuum, **83**, S220–S223, 2009.

18. Z. SWIATEK, M. MICHALEC, N. LEVINTANT-ZAYONTS, J. BONARSKI, A. BUDZIAK, O. BONCHYK, G. SAVITSKIJ, *Structural evolution of near-surface layers in NiTi alloy caused by an ion implantation*, Acta Physica Polonica A, **1**, 75–78, 2011.

19. H. TOBUSHI, K. MITSUI, K. TAKEDA, K. KITAMURA, Y. YOSHIMI, *Performance and design of precision-cast shape memory alloy brain spatula*, J. Theoretical and Appl. Mech., **50**, 3, 855–869, 2012.

20. M. KAWAGUCHI, Y. OHASHI, H. TOBUSHI, *Cyclic characteristics of pseudoelasticity of Ti-Ni alloys: effect of maximum strain, test temperature and shape memory processing temperature*, JSME International Journal, Series I, **34**, 76–82, 1991.

21. H. TOBUSHI, T. NAKAHARA, Y. SHIMENO, T. HASHIMOTO, *Low-cycle fatigue of TiNi shape-memory alloy and formulation of fatigue life*, Trans. ASME, J. Eng. Mater. Tech., **122**, 186–191, 2000.

22. E. PIECZYSKA, S. GADAJ, W.K. NOWACKI, K. HOSHIO, Y. MAKINO, H. TOBUSHI, *Characteristics of energy storage and dissipation in TiNi shape memory alloy*, Sci. Tech. Advanced Mater., **6**, 889–894, 2005.

23. R. MATSUI, Y. MAKINO, H. TOBUSHI, Y. FURUICHI, F. YOSHIDA, *Influence of strain ratio on bending fatigue life and fatigue crack growth in TiNi shape-memory alloy thin wires*, Mater. Trans., **47**, 759–765, 2006.

24. K. TANAKA, T. HAYASHI, Y. ITO, H. TOBUSHI, *Analysis of theremomechanical behavior of shape memory alloys*, Mech. Mater., **13**, 207–215, 1992.

25. W.C. OLIVER, G.M. PHARR, *An improved technique for determining hardness and elastic modulus using load and displacement sensing indentation experiments*, J. Mater. Res., **7**, 1564–1583, 1992.

26. J.E. SHIGLEY, C.R. MISCHKE, *Mechanical Engineering Design*, 5th ed., McGraw-Hill, New York, 1989, 282–283.

Received December 3, 2014; revised version April 3, 2015.